Conference of Bussines, Social Sciences and Technology
59
Vol. 6 Issue 1, 2026, 59-70

Enhanced Structural Stability of $LiMn_{1.9}Ti_{0.1}O_4$ Dysprosium Doping Synthesized by Self Propagating Combustion Method for Li-Ion Batteries

S.A.F. Bakri[1], M.H.H. Mokhtar[2], I. Buniyamin[3], N.A.M. Makhatar[4], A.F.M. Fadzil[5*]

[1-5]Universiti Teknologi MARA, Malaysia
✉ Corresponding email: aidafazliza@uitm.edu.my

History of Article
Submitted : June 30, 2026
Revised : July 22, 2026
Accepted : August 10, 2026
Published : September 22, 2026
DOI : https://doi.org/10.37253/conescintech.v6i1.12711

Copyright© 2026 by Author(s). This work is licensed under a Creative Commons Attribution-Non Commercial-Share Alike 4.0 International License. All writings published in this journal are personal views of the authors and do not represent the views of this journal and the author's affiliated institutions.

Abstract

The spinel-structured material $LiMn_2O_4$ (LMO) has attracted attention for its good rate capability but suffers from capacity fading, manganese dissolution, and poor stability at high temperatures. Partial doping with other elements is an effective strategy to address the issues. To identify suitable dopants ratios for potential cathode material, the structural and morphological is studied through Titanium (Ti) substitution and rare-earth co-doping with dysprosium (x =0.01 and x= 0.05) using Self-Propagating Combustion (SPC) method. The synthesized samples were characterized using X-ray Diffraction (XRD), Scanning Electron Microscopy (SEM) and Energy Dispersive X-ray Spectroscopy (EDX). The XRD profiles show very good fit between the observed data base. The obtained samples were identified as single-phase spinel with a face centred cubic (FCC) structure. The XRD data are also indicates that Dy doping does not affect the formation of the cubic spinel structure of $LiMn_{1.9}Ti_{0.1}O_4$. Annealing at 800℃ for 24 hours causes an increase in sample crystallinity. Scanning Electron Microscopy (SEM) and Energy Dispersive X-ray Spectroscopy (EDX) analyses showed uniformly distributed polyhedral particles ranges between of 0.312 µm until 0.348 µm. These results highlight that partial substitution of Dy into Ti significantly enhances both structural stability and morphological homogeneity as potential cathode material for next-generation lithium-ion batteries.

Keywords: $LiMnTiO_4$; Rare-earth; Dysprosium; Combustion; Lithium-ion batteries

Introduction

The growth of improved cathode materials has increased due to the growing need for high-performance lithium-ion batteries (LIB) for large scale energy storage systems

and electric automobiles. LIBs can store energy and operate well in the standard temperature range of 20–60 ◦C, but performance significantly degrades when the temperature drops below zero (Belgibayeva et al., 2023). Because of its high working voltage (~4.0 V), low cost, environmental friendliness, and three-dimensional lithium-ion diffusion paths that offer outstanding rate capability, spinel lithium manganese oxide ($LiMn_2O_4$) has garnered a lot of attention among the available candidates. However, substantial capacity fading, especially at high temperatures, limits its practical utilization and is mostly caused by Jahn-Teller distortion and manganese dissolution. While the dissolution of manganese into the electrolyte further deteriorates the cathode structure and electrochemical performance, the presence of Mn^{3+} ions cause structural distortion and volume changes within the lattice. While lithium postspinels have been previously found to be thermodynamically stable only at high pressures, we have identified a synthetic pathway that produces the lithium-containing materials at ambient pressure using an ion-exchange process from the corresponding sodium postspinels (Hancock et al., 2024).

Cation substitution has been used extensively to improve the structural stability of LMO to overcome these difficulties. The LMO cathode is mainly plagued by the cubic-tetragonal Jahn Teller distortion, Mn^{2+} dissolution in electrolyte due to the Mn^{3+} disproportionation mechanism, jeopardizes the electrode polarization and long-term cyclability, thus leading to severe capacity degradation upon electrochemical operation (Lin et al., 2025). Furthermore, rare-earth co-doping has become a viable method for enhancing structural integrity. By reducing lattice strain and enhancing resistance to electrolyte attack, dysprosium (Dy^{3+}), with its high ionic radius and concentrated 4f electrons, can function as a structural stabilizer.

However, in the case of doped LiMn2O4 a longer cycle life has been noticed at both room and elevated temperature as well, due to lower capacity loss during charge-discharge cycles, because of the more stable unit cell (Marincaş & Ilea, 2021). Dysprosium is a rare earth element in the row of Lanthanides, which has not been explored as a dopant for cathode materials in lithium-ion batteries (Yan et al., 2020). This study used a combustion approach to create Ti-substituted $LiMn_2O_4$ cathodes co-doped with different Dy concentrations (x = 0.01 and 0.05). Additionally, more fundamental and theoretical research should be conducted on the design of doped lithium manganese oxide spinels to fully utilize the synergistic effects of different doping modes.(Yang et al., n.d.). To assess the efficiency of the Ti–Dy co-doping technique in enhancing the structural stability of spinel cathode materials, the impacts of Dy incorporation on the microstructural and elemental characteristics of $LiMn_{1.9}Ti_{0.1}Dy_xO_4$ were methodically examined.

Experiment Details

Preparation

This study assessed the effects of dysprosium (Dy) substitution on the morphological characteristics and structural stability of Ti-doped lithium manganese

oxide spinel cathodes using a quantitative experimental method. Conversely, cathode materials releasing O2 at high temperatures (>150 ◦C) have been observed to exhibit high reaction rates and enthalpies, favouring inflammation, short-circuiting, and spontaneous battery combustion (Koech et al., 2024). The Self-Propagating Combustion (SPC) process was used to prepared $LiMn_{1.9}Ti_{0.1}Dy_xO_4$ powders and three compositions of $LiMn_{1.9}Ti_{0.1}O_4$ (LMT-10), $LiMn_{1.9}Ti_{0.09}Dy_{0.01}O_4$ (LMTD-01) and $LiMn_{1.9}Ti_{0.05}Dy_{0.05}O_4$ (LMTD-05) were obtained by calculating stoichiometric amounts of the precursor materials.

The sources used were lithium nitrate ($LiNO_3$), manganese nitrate tetrahydrate [$Mn(NO_3)_2 \cdot xH_2O$], titanium precursor, and dysprosium nitrate pentahydrate [$Dy(NO_3)_3 \cdot xH_2O$]. Throughout the synthesis procedure, deionized water with constant stirring was used as the solvent. After that, the precursor solution was mixed with an appropriate combustion agent and gently stirred until a homogenous mixture was created.

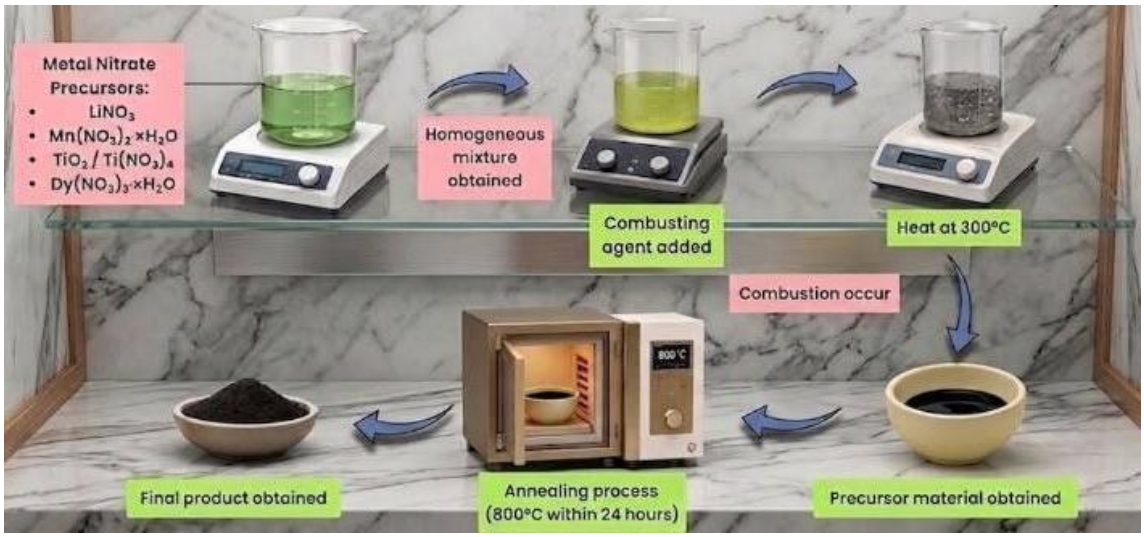


Figure 1: The schematic diagram of precursor preparation for cathode electrode

The selection of the annealing temperature significantly impacts the thermal properties, crystallographic characteristics, specific surface area, and stoichiometric compositions(Lee et al., 2024). A thick gel was created by heating the resultant mixture to 300°C while stirring continuously caused the redox interaction between the nitrate ions and the organic fuel to start a self-sustaining combustion reaction. Along with the production of gaseous byproducts, the combustion process produced a large, porous precursor powder. Solitary sol gel installation can yield materials at ultra-temperatures, synthesize nearly any substance, co-synthesize two or more substances with one other, exactly observance the microstructure of the top outputs, and punctually dominance the physical ،mechanical, and chemical characterizes of the ultimate outputs (Patel et al., 2022).

Heat treatment was performed for 24 hours at 800°C in an ambient air environment in a muffle furnace. The final crystalline spinel products were obtained by allowing the samples to spontaneously cool to ambient temperature following calcination.

Characterization

The synthesized $LiMn_2O_4$ was examined using XRD (Rigaku SmartLab, Cu Kα radiation, λ =1.5406 Å) operated at 40 kV and 40 mA (Uçan et al., 2025). Diffraction data were obtained throughout a 2θ range of 10° to 90°. Diffraction peak resolution is dictated by the properties of the detector and the geometrical resolution of the beamline (Marschilok et al., n.d.).

Scanning Electron Microscopy (SEM) was used to analyse the morphological and microstructural characteristics of the produced samples. Grain properties and particle size were examined at low magnification (1000x) to assess the overall particle distribution.
The elemental composition and distribution of the samples were analysed using Energy Dispersive X-ray Spectroscopy (EDX) coupled with elemental mapping. This technique was employed to determine the quantitative elemental composition, verify the incorporation of Ti and Dy dopants, assess sample purity, and evaluate the spatial distribution of Mn, O, Ti, and Dy within the spinel matrix.

Results and Discussion

X-ray Diffraction (XRD) Structural Analysis

Spinel cathodes constitute an important family of electrode materials for batteries with robust structure, three-dimensional lithium-ion diffusion channel and elevated transition metal redox voltages(Huang et al., 2021). To evaluate the crystal structure, phase purity, and lattice variations of the synthesized materials, X-ray Diffraction (XRD) was carried out. The recorded diffraction profiles for the baseline $LiMn_{1.9}Ti_{0.1}O_4$ (LMT-10), $LiMn_{1.9}Ti_{0.09}Dy_{0.01}O_4$ (LMTD-01), and $LiMn_{1.9}Ti_{0.05}Dy_{0.05}O_4$ (LMTD-05) samples are presented in Figure 4.

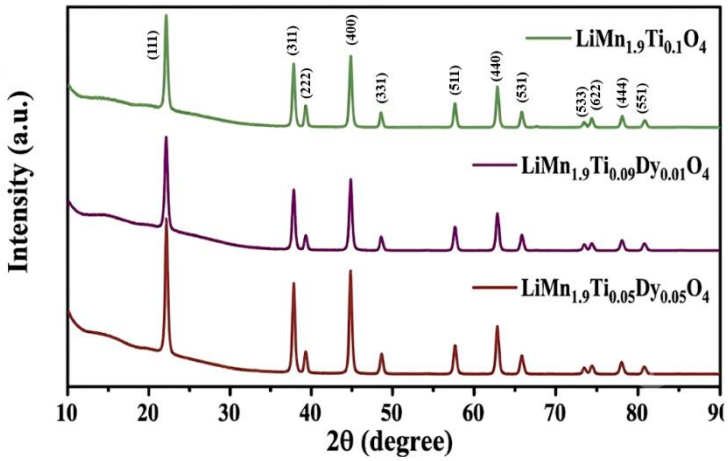


Figure 2: XRD patterns of particles (a) $LiMn_{1.9}Ti_{0.1}O_4$ (LMT-10) (b) $LiMn_{1.9}Ti_{0.09}Dy_{0.01}O_4$ (LMTD-01) and (c) $LiMn_{1.9}Ti_{0.05}Dy_{0.05}O_4$ (LMTD-05)

XRD was carried out for the pre- and post-annealed samples to make certain that high temperature annealing did not affect the substrate itself (Gao, 2020). The distinctive reflection planes of the cubic spinel structure with a $Fd\bar{3}m$ space group symmetry are

precisely matched by the sharp, well-defined peaks in the diffraction profiles for all three compositions. The ideal spinel matrix (111), (311), (400), (511), and (440) Miller indices are represented by prominent reflection peaks seen at 2θ positions around 18.6°, 36.1°, 43.9°, 58.1°, and 63.7°.The crisp reflections for the baseline LMT-10 sample verify that titanium (Ti^{4+}) ions effectively replace the manganese-dominated octahedral 16d sites without disrupting the symmetry of the host framework. By using the Self-Propagating Combustion (SPC) method, no secondary impurity phases, such as unreacted TiO_2 or Mn_2O_3 are found, showing good phase purity.

The fundamental cubic spinel structure is completely maintained when the rare-earth dopant dysprosium is added. There are no distinct reflections or secondary impurity phases associated with dysprosium oxides for either the low-doped LMTD-01 or high-doped LMTD-05 compositions. This suggests that the host crystal structure accommodates the dopant without causing long-range structural disorder or phase breakdown.

A deeper look at the major (111) peak position, it shows that when the dysprosium concentration rises from x = 0.01 to x = 0.05 there is a systematic, slight trend toward lower scattering angles. A downward shift in the diffraction angle indicates a systematic expansion of the interplanar spacing, which raises the unit cell lattice parameter, in accordance with Bragg's Law ($\lambda = 2d \sin\theta$). Direct structural evidence that the bigger cations are integrating into the spinel lattice is provided by this cell expansion. The surrounding oxygen framework widens the interstitial pathways for lithium-ion transport when the bulkier elements partially replace the smaller transition metal ions.

SEM-EDX is a powerful technique for rapid, quantitative, non-destructive, and high-resolution acquisition of effectively all major element chemical information (Guyett et al., 2024). The EDX and SEM observations are in good agreement with these XRD findings. The XRD is an evergreen tool for characterization of materials and the films of past, present and future (Pandey et al., 2021). The absence of distinct impurity peaks in the XRD patterns suggests that these local fluctuations do not disturb the bulk cubic symmetry, even though EDX mapping revealed localized elemental clustering at the higher doping concentration (x = 0.05). Dy doped gradually increases as x becomes larger (Shiwen et al., 2021). Instead, the crystal structure is stabilized by the uniform lattice expansion seen at low-level substitution (x = 0.01). This alteration minimizes structural degradation during high-rate battery cycling by strengthening the octahedral locations, controlling individual grain development, and optimizing the routes for lithium-ion transport.

Scanning Electron Microscopy (SEM) Morphological Analysis.

The morphological evolution of the spinel cathode materials as a function of Dy co-doping concentration was investigated via SEM. To ensure statistical reliability and assess particle size uniformity, individual grain sizes were measured at 1000x magnification. The quantified grain size result for individual randomly selected particles at scale 1µm and their calculated averages in Figure 3.

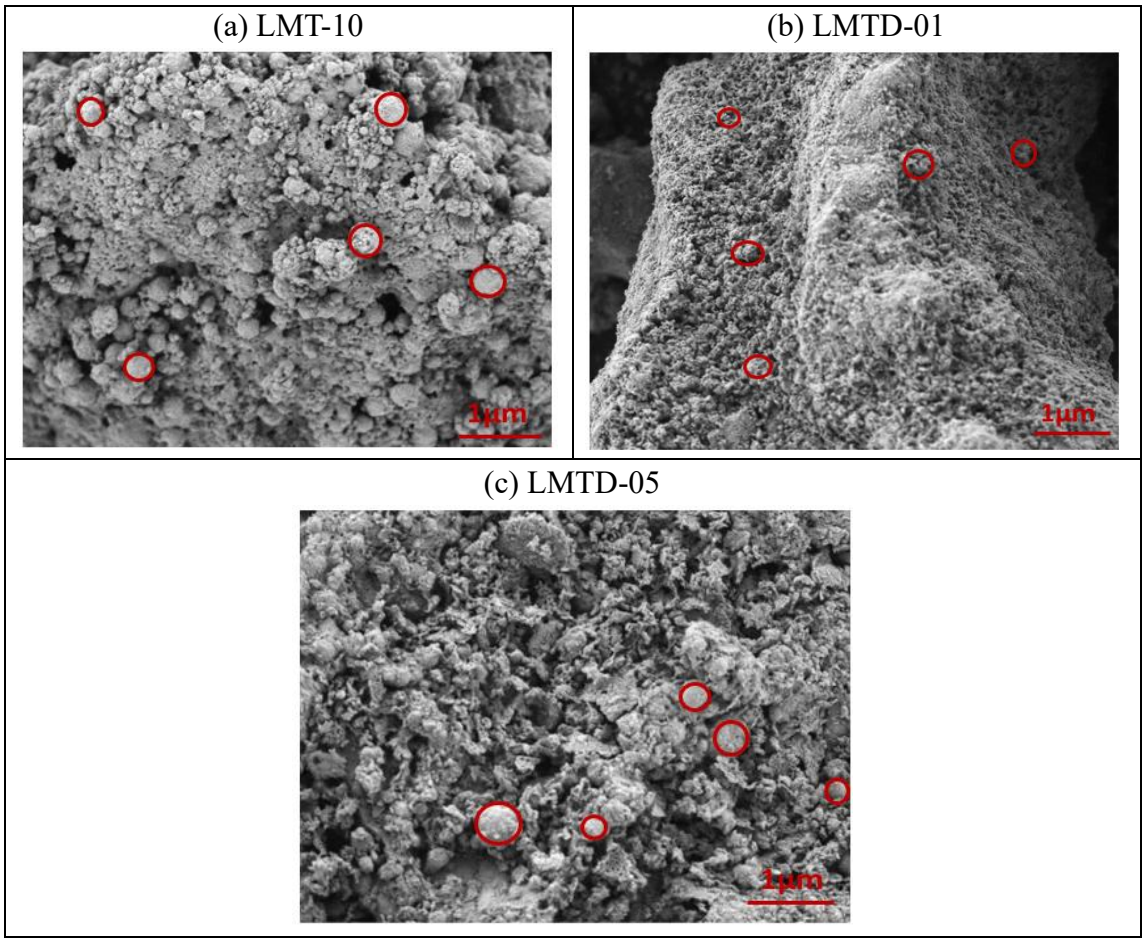


Figure 3: SEM images of (a) LMT-10 (b) LMTD-01 (c) LMTD-05

The average particle size was calculated by determining mean values of the diameters of five representative particles using this formula:

Table 1: The average particle size of LMT-10, LMTD-01 and LMTD-05 samples at magnification 1000x annealed at 800°C for 24 hours

Sample ID	Magnification	Particle 1 (µm)	Particle 2 (µm)	Particle 3 (µm)	Particle 4 (µm)	Particle 5 (µm)	Calculated Average Size (µm)
LMT-10	1000x	0.30	0.38	0.36	0.40	0.30	0.348
LMTD-01	1000x	0.27	0.30	0.35	0.25	0.40	0.314
LMTD-05	1000x	0.49	0.22	0.28	0.33	0.24	0.312

SEM analysis also confirms that particle morphologies remain consistently comparable across all as- synthesized samples (Park et al., 2025). For each SEM micrograph, five typical particles were chosen, and the mean particle size was calculated based on image scale conversion ratio of 1 cm = 1 µm. At 1000x magnification, the baseline LMT-10 samples individual particle sizes range narrowest from 0.30 µm to 0.40 µm, resulting in an average particle size of 0.348 µm. The sample has a baseline level of particle connectedness at this magnification that is characteristics of the combustion

synthesis process, creating linked microstructural frameworks with a rather uniform beginning distribution of sub-micron building blocks.

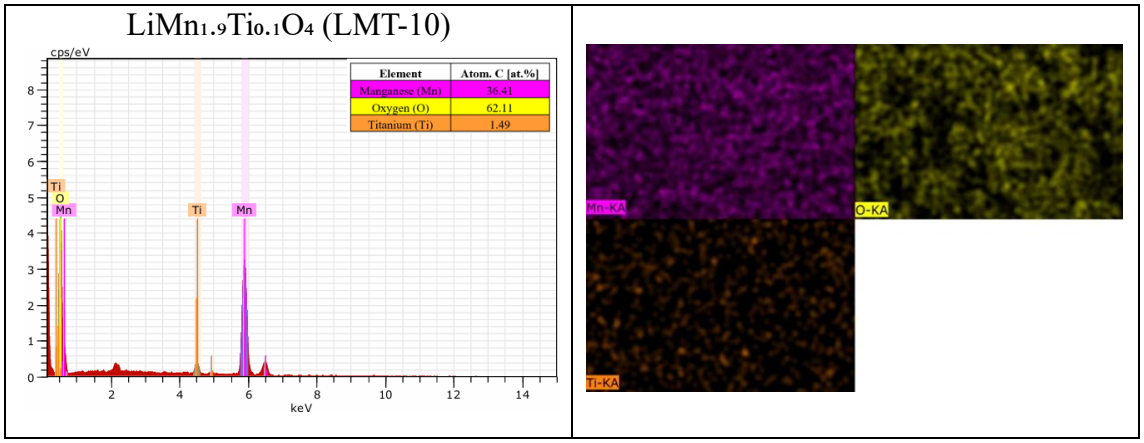
A noticeable change in the bulk morphology is seen when a trace amount of dysprosium co-dopant (x = 0.01) is added to the LMTD-01 sample. At 1000x magnification, the average particle size drops to 0.314 µm, while the boundaries of individual particles range from 0.25 µm to 0.40 µm. The decrease in size at this lower magnification level suggests that during the calcination process, the trace rare-earth elements function as structural inhibitors, limiting broad particle development and clustering across the bulk matrix. The highly faceted, unique truncated octahedrons seen at higher magnifications are directly related to this microstructural modification, which can produce a more refined, disconnected, and loose powder arrangement at low magnification.

The average particle size values obtained at 1000x magnification decrease to their lowest value of 0.312 µm when the dysprosium concentration in the LMTD-05 sample is raised to x = 0.05. This shows the highest suppression of grain growth and the smallest average particle size, indicating that increasing the Dy incorporation can lead to more control over microstructural development.

The microstructure of $LiMn_{1.9}Ti_{0.1}O_4$ (LMT-10) changed as the Dy content increased, resulting in smaller particles and a more uniform distribution, as the SEM data illustrates. Dy-doped $LiMn_{1.9}Ti_{0.1}O_4$ (LMT-10) is a promising cathode material for advanced lithium-ion battery applications because of the morphological changes that enhance lithium-ion diffusion and structural resistance.

Elemental Composition and EDX Mapping Analysis

The EDX analysis of bulk samples may interfere with the compositional characteristic of particles originating from different sources (Bora et al., 2021). EDX spectroscopy confirmed the presence of all constituent heavy elements (Mn, O, Ti, and Dy) within the synthesized samples. Because lithium is too light to be detected by standard EDX (Z = 3), the elemental concentrations focus on the framework metals and oxygen. The EDX spectrum analysis is summarized in Figure 2 below.



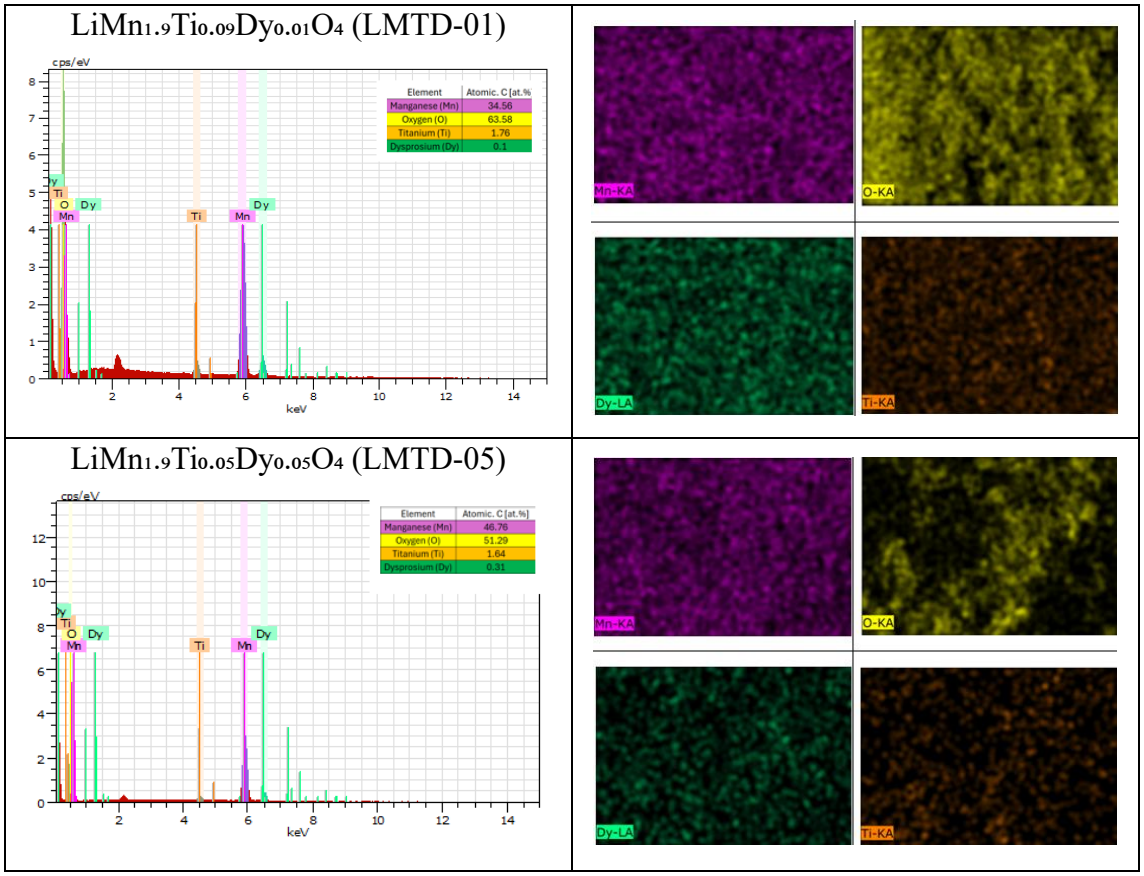


Figure 4: EDX mapping results of (a) LMT-10, (b) LMTD-01, and (c) LMTD-05 particles.

Table 2: Quantitative EDX Elemental Compositions of the Spinel Samples

Sample ID	Chemical Formula	Manganese (Mn) [at.%]	Oxygen (O) [at.%]	Titanium (Ti) [at.%]	Dysprosium (Dy) [at.%]
LMT-10	$LiMn_{1.9}Ti_{0.1}O_4$	36.41	62.11	1.49	-
LMTD-01	$LiMn_{1.9}Ti_{0.09}Dy_{0.01}O_4$	34.56	63.58	1.76	0.10
LMTD-05	$LiMn_{1.9}Ti_{0.05}Dy_{0.05}O_4$	46.76	51.29	1.64	0.31

EDX spectroscopy also helped the current study in exploring the elemental distribution inside the adhesive (Alqarawi et al., 2021). The baseline (a) $LiMn_{1.9}Ti_{0.1}O_4$ (LMT-10) sample EDX shows that the prominent characteristic peaks that only corresponds to manganese (Mn), oxygen (O), and titanium (Ti), indicating the successful formation of the pristine transition metal-doped lithium manganese oxide material. The great chemical purity of the synthesized sample was confirmed by the absence of any additional impurity related peaks within the spectral resolution limits. The distinctive peaks associated with the rare-earth element dysprosium (Dy) are clearly seen for co-doped compositions. Dy is measured at a trace amount in the low doped (b) $LiMn_{1.9}Ti_{0.09}Dy_{0.01}O_4$ (LMTD-01) samples, which scales proportionately to in the higher

doped (c) $LiMn_{1.9}Ti_{0.05}Dy_{0.05}O_4$ (LMTD-05) configuration, demonstrating the successful implementation across different designed doping levels.

At modest levels of rare earth substitution, the measured transition metal to oxygen ratios stay near the nominal values predicted for a well-coordinated spinel structure, suggesting that oxygen coordination and compositional balance within the host crystal framework are mainly maintained. Nevertheless, the corresponding elemental maps shows localized regions where the concentration of Dy is significantly higher than the surrounding matrix when the dysprosium content is increase to (c) $LiMn_{1.9}Ti_{0.05}Dy_{0.05}O_4$ (LMTD-05). This illustrates how local enrichment and segregation during crystal formation and high temperature thermal processing cause the element distribution to become less uniform at higher co-doping thresholds. Previous structural analyses showed no phase separation in the bulk crystal despite this localized enrichment, indicating that the primary cubic spinel symmetry is still there.

The structural and morphological behaviour shown in all the samples is directly correlated with these trends in elemental distribution. The LMTD-01 composition's remarkable spatial homogeneity is consistent with refined grain boundaries and a stable cubic framework. Controlled grain worth combined with homogeneity is consistent with refined grain boundaries and a stable cubic framework. Controlled grain growth combined with homogeneous dopant integration suggest that low level substitution with Dy stabilizes the host microstructure. On the other hand, increasing the rare earth substitution causes more local compositional changes, which may cause uneven grain aggregation and disturb the uniform lattice fields. For advanced lithium-ion battery applications, the LMTD-01 structure thus creates the best possible compromise between compositional uniformity, structural stability, and microstructural refinement.

Conclusion

In conclusion, the direct evidence between the mechanical responses beneath the indenter and the localized characteristics of indents confirmed that the nanoscale mechanical properties are compositional and microstructural dependent (Liu et al., 2022). Sol–gel syntheses were attempted using annealing conditions similar to the one used for the synthesis of the spinel-based active materials. (Callegari et al., 2022). Self-Propagating Combustion (SPC) approach was effectively used to synthesis a variety of Ti and Dy doped spinel cathode materials, $LiMn_2O_4$ (x = 0.01, 0.01, 0.05). The successful incorporation of Ti and Dy into the host lattice was demonstrated by X-ray diffraction analysis, which verified that all synthesized samples maintained a highly crystalline cubic spinel structure and had no discernible secondary phases. As the Dy concentration increased, the (111) diffraction peak gradually shifted toward lower diffraction angles, indicating lattice expansion as the bigger Dy^{3+} ions replaced the transition metal ions. By expanding the interstitial routes inside the spinel framework, tis structural alteration is anticipated to promote lithium-ion transport.

According to the microstructural analysis, it revealed that Dy presence affected grain development during calcination. The LMTD-05 sample had the least average particle size of 0.312 µm, compared to 0.348 µm for LMT-10 and 0.314 µm for LMTD-

01. SEM studies revealed a decrease in particles for electrochemical performance. The lack of structural degradation in the XRD patterns shows that the cubic spinel framework remained robust despite the increased dopant content, even though EDX examination revealed modest elements clustering at the maximum Dy concentration.

Thus, the results show that Dy co doped successfully alters the microstructure and crystal structure of Ti substituted $LiMn_2O_4$. the LMTD-05 sample showed the smallest particle morphology and the largest lattice expansion among the synthesized compositions, indicating that this composition offers improved structural properties for possible high-performance lithium-ion battery cathode applications. To determine the connection between these structural enhancements and battery performance, more electrochemical research is needed.

References

Alqarawi, F. K., Alkahtany, M. F., Almadi, K. H., Ben Gassem, A. A., Alshahrani, F. A., Alrefeai, M. H., Farooq, I., Vohra, F., & Abduljabbar, T. (2021). Influence of different conditioning treatments on the bond integrity of root dentin to rgo infiltrated dentin adhesive. Sem, edx, ftir and microraman study. *Polymers*, *13*(10). https://doi.org/10.3390/polym13101555

Belgibayeva, A., Rakhmetova, A., Rakhatkyzy, M., Kairova, M., Mukushev, I., Issatayev, N., Kalimuldina, G., Nurpeissova, A., Sun, Y. K., & Bakenov, Z. (2023). Lithium-ion batteries for low-temperature applications: Limiting factors and solutions. In *Journal of Power Sources* (Vol. 557). Elsevier B.V. https://doi.org/10.1016/j.jpowsour.2022.232550

Bora, J., Deka, P., Bhuyan, P., Sarma, K. P., & Hoque, R. R. (2021). Morphology and mineralogy of ambient particulate matter over mid-Brahmaputra Valley: application of SEM–EDX, XRD, and FTIR techniques. *SN Applied Sciences*, *3*(1). https://doi.org/10.1007/s42452-020-04117-8

Callegari, D., Coduri, M., Fracchia, M., Ghigna, P., Braglia, L., Anselmi Tamburini, U., & Quartarone, E. (2022). Lithium intercalation mechanisms and critical role of multi-doping in LiFexMn2−x−yTiyO4 as high-capacity cathode material for lithium-ion batteries. *Journal of Materials Chemistry C*, *10*(23), 8994–9008. https://doi.org/10.1039/d2tc00573e

Gao, Y. (2020). *Scholars' Mine Scholars' Mine Enhanced electrochemical performance of Li-ion battery cathodes Enhanced electrochemical performance of Li-ion battery cathodes by atomic layer deposition by atomic layer deposition*. https://scholarsmine.mst.edu/doctoral_dissertations/3074

Guyett, P. C., Chew, D., Azevedo, V., Blennerhassett, L. C., Rosca, C., & Tomlinson, E. (2024). Optimizing SEM-EDX for fast, high-quality and non-destructive elemental analysis of glass. *Journal of Analytical Atomic Spectrometry*, *39*(10), 2565–2579. https://doi.org/10.1039/d4ja00212a

Hancock, J. C., Ding, P. P., Choi, Y., Ceder, G., Vaughey, J. T., Griffith, K. J., & Poeppelmeier, K. R. (2024). Electrochemistry in the Large Tunnels of Lithium

Postspinel Compounds. *Chemistry of Materials*, *36*(9), 4616–4630. https://doi.org/10.1021/acs.chemmater.4c00389

Huang, Y., Dong, Y., Li, S., Lee, J., Wang, C., Zhu, Z., Xue, W., Li, Y., & Li, J. (2021). Lithium Manganese Spinel Cathodes for Lithium-Ion Batteries. In *Advanced Energy Materials* (Vol. 11, Number 2). Wiley-VCH Verlag. https://doi.org/10.1002/aenm.202000997

Koech, A. K., Mwandila, G., Mulolani, F., & Mwaanga, P. (2024). Lithium-ion battery fundamentals and exploration of cathode materials: A review. In *South African Journal of Chemical Engineering* (Vol. 50, pp. 321–339). Elsevier B.V. https://doi.org/10.1016/j.sajce.2024.09.008

Lee, S. H., Cha, H. J., Park, J., Son, C. S., Son, Y. G., & Hwang, D. (2024). Effect of Annealing Temperature on the Structural and Electrochemical Properties of Hydrothermally Synthesized NiCo2O4 Electrodes. *Nanomaterials*, *14*(1). https://doi.org/10.3390/nano14010079

Lin, X., Lin, J., Lu, X., Tan, X., Li, H., Mai, W., Luo, Y., Wu, Y., Chen, S., Yang, C., & Wang, Y. (2025). Vacancy-engineered LiMn2O4 embedded in dual-heteroatom-doped carbon via metal-organic framework-mediated synthesis towards longevous lithium ion battery. *Materials Futures*, *4*(2). https://doi.org/10.1088/2752-5724/ad9e08

Liu, A., Liu, S., Liu, Y., Liu, B., & Liu, T. (2022). Characterizing mechanical heterogeneity of coal at nano-to-micro scale using combined nanoindentation and FESEM-EDS. *International Journal of Coal Geology*, *261*. https://doi.org/10.1016/j.coal.2022.104081

Marincaş, A. H., & Ilea, P. (2021). Enhancing lithium manganese oxide electrochemical behavior by doping and surface modifications. In *Coatings* (Vol. 11, Number 4). MDPI AG. https://doi.org/10.3390/coatings11040456

Marschilok, A. C., Bruck, A. M., Abraham, A., Stackhouse, C. A., Takeuchi, K. J., Takeuchi, E. S., Croft, M., & Gallaway, J. W. (n.d.). Energy dispersive X-ray diffraction (EDXRD) for operando materials characterization within batteries Article Type: Perspective Energy dispersive X-ray diffraction (EDXRD) for operando materials characterization within batteries. In *Journal: Physical Chemistry Chemical Physics*.

Pandey, A., Dalal, S., Dutta, S., & Dixit, A. (2021). Structural characterization of polycrystalline thin films by X-ray diffraction techniques. In *Journal of Materials Science: Materials in Electronics* (Vol. 32, Number 2, pp. 1341–1368). Springer. https://doi.org/10.1007/s10854-020-04998-w

Park, S. W., Kim, H., Han, S., Kim, K. S., Song, Y. Y., Lee, H. G., Jang, W., Lee, D. H., Bae, S., Kim, D., Park, J., Park, I., Nam, S. C., Kim, H., Lee, J., Kang, K., & Seo, D. H. (2025). High-Throughput Synthesis of Mn-Based Disordered Rock-Salt Li-Ion Cathodes with Improved Rate Capability via Rapid Joule-Heating. *Advanced Energy Materials*. https://doi.org/10.1002/aenm.202503496

Patel, M., Mishra, S., Verma, R., & Shikha, D. (2022). Synthesis of ZnO and CuO nanoparticles via Sol gel method and its characterization by using various

technique. *Discover Materials* , *2*(1). https://doi.org/10.1007/s43939-022-00022-6

Shiwen, L., Jiatong, P., Feng, G., Deqian, Z., Qin, F., Chunling, H., Dodbiba, G., Wei, Y., & Fujita, T. (2021). *Structure and magnetic properties of coprecipitated nickel-zinc ferrite doped rare earth elements of Sc, Dy, and Gd*. https://doi.org/10.21203/rs.3.rs-277352/v1

Uçan, M., ōzgenç, D., Topcu, Y., & Tekin, B. (2025). First-Ever Use of $LiMn_2O_4$ Cathode in State-of-the-Art Ammonium-Ion Batteries: Unlocking a New Ametal Charge Carrier. *Erzincan Üniversitesi Fen Bilimleri Enstitüsü Dergisi*, *18*(2), 431–450. https://doi.org/10.18185/erzifbed.1673054

Yan, C., Yang, X., Zhao, H., Zhong, H., Ma, G., Qi, Y., Koel, B. E., & Ju, Y. (2020). *Controlled Dy-doping to Nickel-rich Cathode Materials in High Temperature Aerosol Synthesis*.

Yang, Y., Shi, L., & Guo, J. (n.d.). *Structure and electrochemical properties of Mg-Al co-doped spinel LiMn 2 O 4 cathode material*. Retrieved https://ssrn.com/abstract=5334765